

High-field 1/f noise in hBN-encapsulated graphene transistors

A. Schmitt,^{1,*} D. Mele,^{1,2} M. Rosticher,¹ T. Taniguchi,³ K. Watanabe,³ C. Maestre,⁴ C. Journet,⁴ V. Garnier,⁵ G. Fève,¹ J.M. Berroir,¹ C. Voisin,¹ B. Plaçais,^{1,†} and E. Baudin^{1,‡}

¹*Laboratoire de Physique de l'Ecole normale supérieure,
ENS, Université PSL, CNRS, Sorbonne Université,
Université de Paris, 24 rue Lhomond, 75005 Paris, France*

²*Univ. Lille, CNRS, Centrale Lille,
Univ. Polytechnique Hauts-de-France, Junia-ISEN,
UMR 8520-IEMN, F-59000 Lille, France.*

³*Advanced Materials Laboratory, National Institute for
Materials Science, Tsukuba, Ibaraki 305-0047, Japan*

⁴*Laboratoire des Multimatériaux et Interfaces, UMR CNRS 5615, Univ Lyon,
Université Claude Bernard Lyon 1, F-69622 Villeurbanne, France*

⁵*Université de Lyon, MATEIS, UMR CNRS 5510,
INSA-Lyon, F-69621 Villeurbanne cedex, France*

Abstract

Low-frequency $1/f$ noise in electronics is a conductance fluctuation, that has been expressed in terms of a mobility "α-noise" by Hooge and Kleinpenning. Understanding this noise in graphene is a key towards high-performance electronics. Early investigations in diffusive graphene have pointed out a deviation from the standard Hooge formula, with a modified expression where the free-carrier density is substituted by a constant density $n_{\Delta} \sim 10^{12} \text{ cm}^{-2}$. We investigate hBN-encapsulated graphene transistors where high mobility gives rise to the non-linear velocity-saturation regime. In this regime, the α-noise is accounted for by substituting conductance by differential conductance G , resulting in a bell-shape dependence of flicker noise with bias voltage V . The same analysis holds at larger bias in the Zener regime, with two main differences: the first one is a strong enhancement of the Hooge parameter reflecting the hundred-times larger coupling of interband excitations to the hyperbolic phonon-polariton (HPhP) modes of the mid-infrared Reststrahlen (RS) bands of hBN. The second is an exponential suppression of this coupling at large fields, which we attribute to decoherence effects. We also show that the HPhP bands control the amplitude of flicker noise according to the graphene-hBN thermal coupling estimated with microwave noise thermometry. The phenomenology of α-noise in graphene supports a quantum-coherent bremsstrahlung interpretation of flicker noise.

Flicker ($1/f$) noise is a type of noise that dominates the spectral density at low frequencies. Ubiquitous in condensed matter and quantum conductors, it has also been measured in a large variety of systems ranging from biology to economics. In electronics, flicker noise is a conductance fluctuation revealed as an excess low-frequency current noise, of spectral density $S_I = CI^2/f$, superimposed on the Johnson-Nyquist thermal noise $S_{th} = 4Gk_B T$ at finite bias current I . Despite almost a century of research on $1/f$ noise since Johnson measured it in vacuum tubes [3], its origin remains controversial. In semiconductors, $1/f$ noise is usually well described using the McWorther model relying on carrier number fluctuations due to defect traps [1,2]. Alternative mechanisms based on carrier-number-fluctuation or involving fluctuations of mobility have been proposed. As pointed out by Hooge and Kleinpenning [4], the noise amplitude C is a bulk effect that can be conveniently expressed in terms of a mobility noise, called α -noise, with an intensive Hooge parameter $\alpha_H = NC$, where N is the number of carriers participating to the conductance. Measurements in both metals [5] and semiconductors [6] have yielded a quasi-universal Hooge parameter $\alpha_H \sim 2 - 5 \times 10^{-3}$. A leading interpretation of the α -noise relies on a distribution of two-level fluctuators that locally and elastically modulate electronic transmission [6,7]. An alternative interpretation, based on a quantum theory proposed by Handel [8,9], points to an infrared (IR) bremsstrahlung origin which leads to a $1/f$ noise spectrum with a universal $\alpha_H = 2\alpha_0/\pi = 4.6 \times 10^{-3}$ in the quantum-coherent regime, where $\alpha_0 = 1/137$ is the vacuum fine-structure constant that controls light-matter coupling. This interpretation puts emphasis on an inelastic origin of conductance noise; a critical discussion can be found in Refs.[10,11]. These contrasted interpretations take root in the ambivalent nature of conductivity, which is both a momentum relaxation coefficient $\sigma_1(t) = (J/E)(t)$, and an energy relaxation parameter in the Joule power density $\sigma_2(t) = (P/E^2)(t)$. Whereas $\sigma_1 = \sigma_2$ in average, they may differ in their time dependencies due to different scattering mechanisms and times, fingerprinted in a low-frequency noise $\delta\sigma(t)$.

Graphene is an attractive platform for flicker noise investigation because of the tunability of charge carrier density and polarity. This versatile material also presents strong potential for electronics [12] for which flicker noise is an important performance limit [13]. Most experiments so far have been carried out at low to moderate bias with a $1/f$ corner frequency, separating the low-frequency $1/f$ noise from the high-frequency thermal white noise, in the sub-MHz range [14,15], and mostly on SiO₂-supported devices with a low mo-

bility $\mu \lesssim 0.1 \text{ m}^2/\text{Vs}$. Flicker noise in these diffusive graphene transistors was characterized by a doping-independent flicker amplitude $A = fS_I/I^2LW \in [10^{-7}, 10^{-6}] \text{ } \mu\text{m}^2$ [12] (or $[0.1, 1] \text{ nm}^2$), where L and W the length and width of the graphene channel. This doping-independent value for graphene violates the Hooge empirical formula where $A = \alpha_H/n$ is assumed to be inversely proportional to carrier density n , based on the assumption that electrons behave independently. It can be re-conciliated with a collective picture on substituting n by a constant density n_Δ , which origin remains to be clarified. Some reports also point to a flicker noise dip at charge neutrality [15,16], but charge neutrality corresponds to a non-local mesoscopic regime that deviates from standard local-transport α -noise conditions. The same occurs under intense magnetic fields, with a field-induced noise reduction [17], leading to a full suppression enforced by conductance quantization [18]. Flicker noise suppression was also recently reported in the different system of a break-junction, where it is found to accompany shot-noise suppression at full transmission [19]. A deviation from the above $A = Cte$ diffusive graphene flicker noise was reported in moderate-mobility suspended samples, where a noise reduction was observed [20].

The high-mobility hBN-encapsulated graphene transistors investigated in the present work constitute a testbed for α -noise as they allow studying flicker noise in an extended electric-field range where different scattering and relaxation mechanisms succeed one another in increasing bias. In the perspective of testing the bremsstrahlung interpretation, the use of hBN-encapsulates is an additional asset, as hBN not only provides a superior mobility [25], but also a very characteristic mid-infrared (MIR) near-field electromagnetic environment [26,27], with its two Reststrahlen (RS) bands, $\hbar\Omega_I = 95\text{-}100 \text{ meV}$ and $\hbar\Omega_{II} = 170\text{-}200 \text{ meV}$. As a matter of fact, recent experiments have shown that the hyperbolic light of these RS bands strongly couples to graphene electronic transport [22,23]. The three electronic transport regimes observed in increasing electric field are: (i) the mobility-limited Drude regime $J = \sigma E = ne\mu E$ at low field, (ii) the velocity saturation regime for $E \gtrsim E_{sat} = v_{sat}/\mu$ where v_{sat} is the phonon-limited saturation velocity, and finally (iii) the interband Zener regime characterized by a doping and bias-independent differential conductivity σ_Z . Based on combined transport, flicker and thermal noise characterization in a series of high-quality samples, we show that : i) the standard analysis of flicker noise in graphene can be consistently extended to the non-linear saturation regime and, ii) the interband Zener contribution of gapless graphene can be accounted for by introducing a semi-empirical formula in the spirit

of the bremsstrahlung interpretation, accounting for the enhanced electromagnetic coupling of interband excitations and decoherence effects.

We use a series of ten hBN-encapsulated graphene transistors, of a large size $(L, W) = 4 - 25 \mu\text{m}$ and low edge-contact resistance R_c , exhibiting varied but large mobility $\mu = 2 - 15 \text{ m}^2/\text{Vs}$, saturation velocity $v_{sat} = 0.2-0.8v_F$, and Zener conductivity $\sigma_Z = 0.1-1 \text{ mS}$, as described in Supplementary Table-SI-1. They map a broad range of hBN dielectric thickness $t_{hBN} = 50 - 160 \text{ nm}$ and a variety of gating: (IR reflecting) Au bottom gates, (IR absorbing) graphite bottom gates or SiO_2 -insulated Si back gates. We also use two different hBN grades: the high-pressure high-temperature (HPHT) from NIMS [28], and the polymer-derived ceramic (PDC) from Lyon [29,30] which behave differently. All devices are embedded in coplanar waveguides for room-temperature probe-station measurement of DC transport, sub-MHz flicker noise, and microwave thermal noise (see Fig. 1-a). Thanks to their high mobility, transistors sustain large saturation currents ($\sim 1 \text{ mA}/\mu\text{m}$), rejecting the $1/f$ noise corner frequency ($f_c = CI^2/4Gk_B T \propto I$) in the low GHz range. As a matter of fact, the flicker noise tails are visible in the GHz noise spectra and allow for a sanity check of the sub-MHz measurements.

Current noise is analyzed with a modified Hooge formula $S_I = C(GV)^2/f$, obtained by substituting the total DC current I by the differential current GV to account for non-linear transport [24]. Here V is the drain-source voltage obtained after subtraction of the contact-voltage drop ($R_c I$), $G = (ne\mu(E) + \sigma_Z)W/L$ is the differential conductance with $\mu(E) = \mu(0)/(1+E/E_{sat})^2$ the optical phonon-limited mobility with E_{sat} and $v_{sat} = \mu(0)E_{sat}$ the saturation field and velocity. Following Ref.[22], we correct for drain-gating effect by biasing transistors along constant density lines on applying a bias-dependent gate voltage $V_g(V) = V_g(0) + \beta V$. This biasing procedure allows rejecting drain pinch-off effect, such as investigated in Ref.[31], while securing quasi-homogeneous doping and electric fields, up to small gradients that become negligible at large doping. Low-frequency noise characterization is enriched by Johnson-Nyquist thermal noise measurements, performed in the microwave (1-10 GHz) band where flicker noise contribution is negligible [22]. This allows estimating the electronic temperature T_N and extract the thermal conductivity dP/dT_N to the hBN substrate which turns on in the Zener regime [23], where $P = VI/LW$ is the areal Joule power.

Figure 1 summarizes the experimental technique (panel a) and procedure (panels b-d).

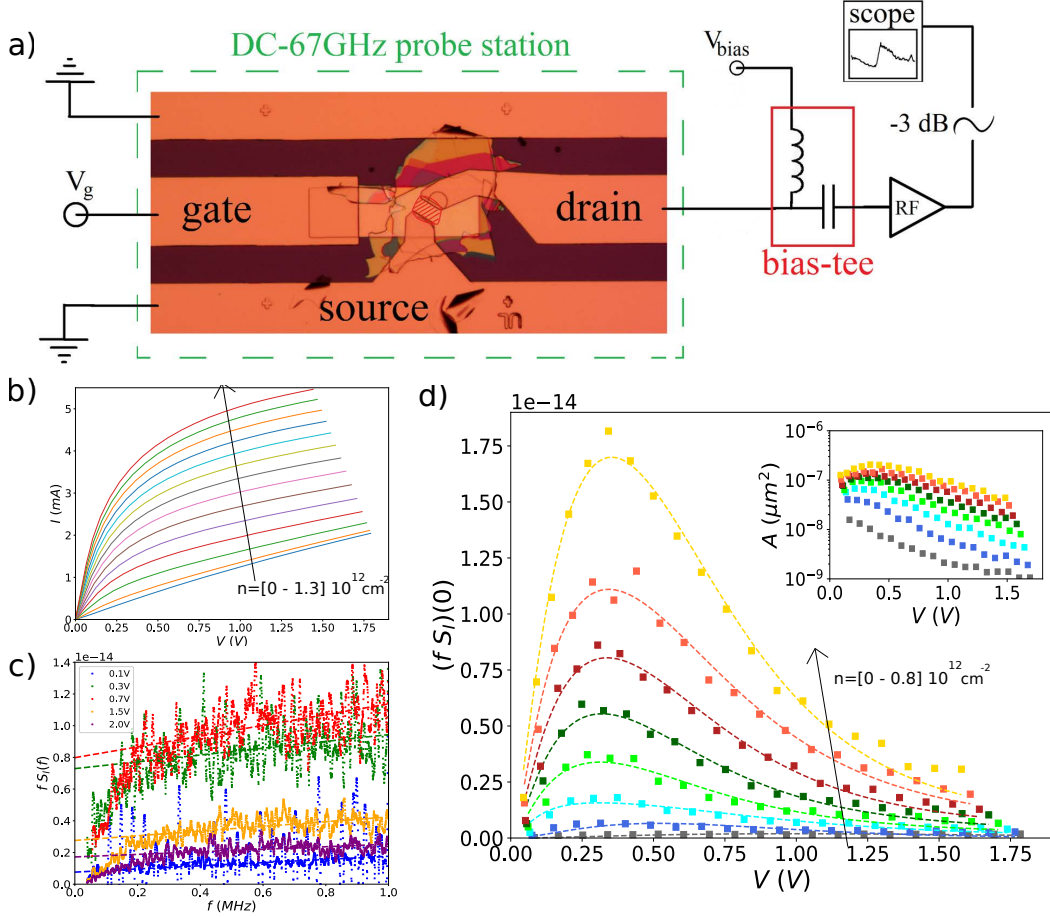


FIG. 1: DC transport and flicker noise in the high-mobility graphene transistor GRS5. a) Experimental setup for low-frequency and GHz noise measurements, with the graphene transistor embedded in a coplanar waveguide. b): current-voltage curves for doping $n = [0 - 1.3]10^{12} \text{ cm}^{-2}$ corresponding to a Fermi energy $\epsilon_F = [0 - 130] \text{ meV}$. c): Noise spectra in increasing bias at $n = 0.6 \times 10^{12} \text{ cm}^{-2}$. Flicker noise appears as plateaus of $fS_I(f)$. Dashed lines are linear fits of $fS_I(f)$ of the data with slopes and extrapolates $(fS_I)(0)$ measuring respectively the white noise and flicker noise. The fall down of noise below 0.2 MHz is due to the cut-off frequency of the bias-tee. d): bell-shape dependence of $fS_I(0)$ versus V for $n = [0 - 0.8]10^{12} \text{ cm}^{-2}$; inset shows a semi-log plot of $A = fS_I/(GV)^2LW$ for same doping values indicating an exponential decay of A with bias.

Figure 1-b shows typical current-voltage curves measured in the typical transistor “GrS5”. They show the successive low-bias linear ohmic behavior, the velocity-saturation regime for $V > V_{\text{sat}} \simeq 0.25 \text{ V}$, and finally the interband Zener regime. The saturation of intraband

current can be consistently attributed to the scattering by the optical phonons of the lower Reststrahlen (RS) band of hBN ($\hbar\Omega_I = 95-100$ meV) [22]. The Zener regime is accompanied by the onset of energy relaxation by optical phonons of the upper RS band of hBN ($\hbar\Omega_{II} = 170 - 200$ meV) [22]. Its main signature is electron cooling, that is observed in the noise temperature (inset of Fig.3-c) by a decrease of the temperature-field slope. This change of slope is typical of single-layer graphene; in bilayer graphene this radiative cooling is even more drastic and eventually takes the form of a temperature drop with bias [23].

The differential conductivity (not shown) is accurately fitted using the sum of saturation (σ_{sat}) and Zener (σ_Z) contributions [22,32] :

$$\sigma(E) = ne \frac{\mu(0)}{(1 + E/E_{sat})^2} + \sigma_Z \quad , \quad (1)$$

where $\mu(0)$ is the extrapolated low-bias electronic mobility, n is the carrier density, and $E = V/L$. $\mu(0)$ agrees with standard mobility μ deduced from the low-bias $G(V_g)$ dependence. $G = \sigma W/L$, and its constituents G_{sat} (or σ_{sat}) and G_Z (or σ_Z), are the associated differential conductance (conductivity). Eq.(1) is used to extract DC transport parameters $\mu(0)$, E_{sat} or $v_{sat} = \mu(0)E_{sat}$ that are listed in Table-SI1.

For each bias and doping, we measure the current noise in the $f = [0.1 - 1]$ MHz frequency band, as shown in Fig.1-c. Flicker $1/f$ noise corresponds to plateaus $fS_I(f) = a + bf$, where a is the amplitude of flicker noise and b measures the instrumental background noise. The α -noise amplitude a (denoted $fS_I(0)$ in Fig.1-d and thereafter) has an asymmetric bell-shape bias dependence, and a strong doping dependence $fS_I \propto n^2$. The noise amplitude $A = fS_I/(GV)^2(WL)$ is plotted in the inset of Fig.1-d. Its low-bias extrapolate $A \sim 10^{-7} \mu\text{m}^2$ is consistent with diffusive graphene values [12]. At high bias we observe an amplitude suppression, with A dropping below $10^{-8} \mu\text{m}^2$, following an exponential dependence $A \propto e^{-E/E_\Lambda}$ (inset of Fig.1-d), with a characteristic electric field $E_\Lambda \sim 0.1$ V/ μm . The doping dependence $fS_I \propto n^2$ is quite generic; it suggests a doping-independent velocity flicker noise, $fS_v LW = Av^2$ (with $v = \mu(E)E$), as illustrated in Supplementary Information Fig.SI-2.

We start our analysis by focusing on the velocity saturation regime, which is exemplified in sample ‘‘Lyon1’’ where the Zener contribution to transport is minimized to $\sigma_Z \simeq 0.1$ mS (Table SI-1), as deduced from the fitting of the differential conductance with Eq.(1) in Fig.2-a data. Consistently, noise thermometry (inset of Fig.2-a) shows little fingerprint of Zener cooling, as opposed to other samples where Zener cooling shows up as a prominent breakout

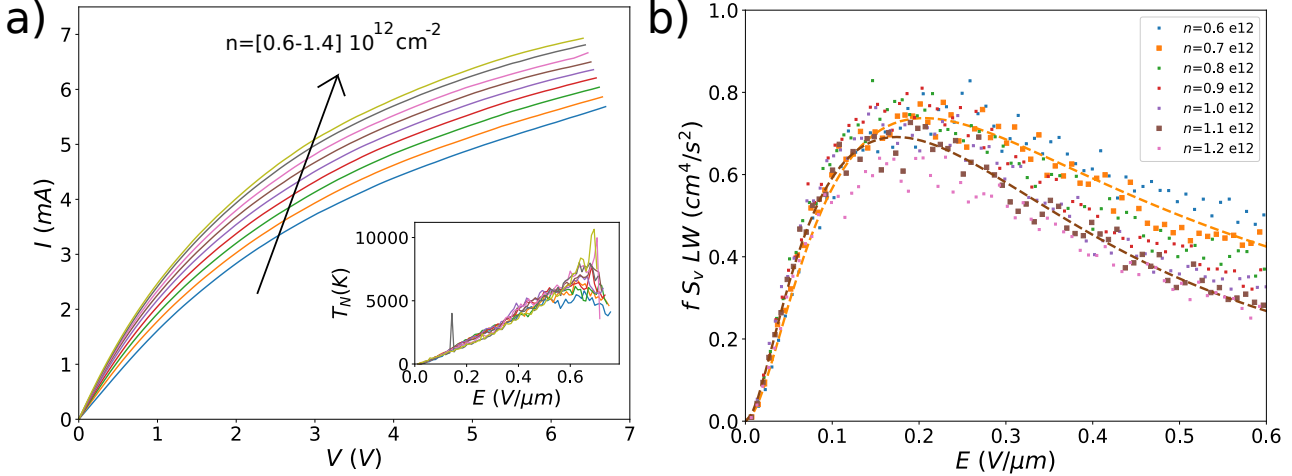


FIG. 2: DC transport and flicker noise in the high-mobility graphene transistor “Lyon1”. a): current-voltage curves, for doping $n = [0.6 - 1.4]10^{12} \text{ cm}^{-2}$, and noise thermometry (inset) show no fingerprint of Zener tunneling and cooling. b): Quasi-scaling of the velocity flicker noise $f S_v LW(E)$ as a function of electric field $E = V/L$. The representative $n = 0.7 \cdot 10^{12} \text{ cm}^{-2}$ (resp. $n = 1.1 \cdot 10^{12} \text{ cm}^{-2}$) data are well fitted by Eq.(2) with $A = 6.4 \cdot 10^{-7} \mu\text{m}^2$ and $v_{sat} = 0.82 v_F$ (resp. $A = 4.6 \cdot 10^{-7} \mu\text{m}^2$ and $v_{sat} = 0.65 v_F$).

of the $T_N(E)$ dependence (see Supplementary Informations Fig.SI-3). The origin of Zener transport suppression in sample “Lyon1” is discussed below. Importantly, the flicker noise in Fig.2-b reduces to its velocity-saturation contribution $f S_{sat} LW = A[\mu(E)E]^2$, which is entirely determined by the differential mobility $\mu(E)$, according to

$$f S_{sat} LW = A \times v_{sat}^2 \left[\frac{E/E_{sat}}{(1 + E/E_{sat})^2} \right]^2. \quad (2)$$

Velocity-flicker in Eq.(2) has a quadratic low-bias onset $f S_{sat} LW = A(\mu(0)E)^2$, consistent with standard Hooge law $f S_I LW = A(I)^2$, a peak $f S_{sat} LW = Av_{sat}^2/16$ at $E = E_{sat}$, and a bias tail $f S_{sat} LW = Av_{sat}^2(E_{sat}/E)^2$. Orange and brown dashed lines in Fig.2-b are theoretical fits with Eq.(2) of the $n = 0.7$ and $n = 1.1 \cdot 10^{12} \text{ cm}^{-2}$ data. The quasi-scaling observed here (and in Figs.SI-2 for the other samples) relies on the weak doping-dependence of v_{sat} (and $E_{sat} = v_{sat}/\mu(0)$ as $\mu(0)$ is doping independent). From the amplitude of the $n = 7 \cdot 10^{11} \text{ cm}^{-2}$ data we deduce $A \simeq 6.4 \cdot 10^{-7} \mu\text{m}^2$ which is indeed consistent with diffusive-graphene literature data [12]. Setting $A = 2\alpha_0/\pi n_{\Delta}$ according to the modified Hooge-Handel formula, we infer $n_{\Delta} \simeq 0.7 \cdot 10^{12} \text{ cm}^{-2}$.

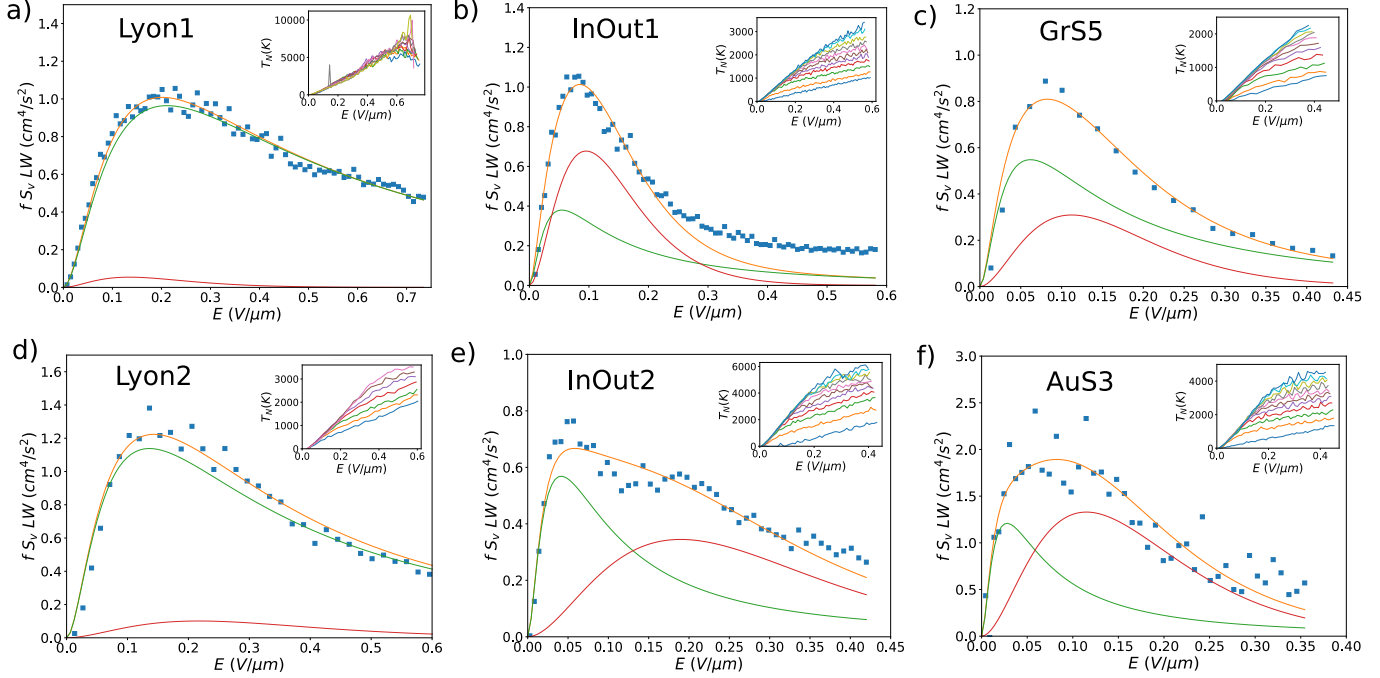


FIG. 3: Velocity flicker noise $fS_v LW$ for 6 typical devices at a representative doping $n = 6 \cdot 10^{11} \text{ cm}^{-2}$ (dots), and their fits with Eqs.(2) and (3) for the two-fluid model. Green and red lines correspond to the saturation and Zener contributions respectively, and the orange lines correspond to their sum. Successive panels correspond to devices of increasing mobility $\mu = 4 \rightarrow 15 \text{ m}^2/\text{Vs}$ (see Table SI-1). Values of the fitted parameters A and E_Λ are summarized in Table SI-1. Insets show for each device the noise temperature T_N as function of bias and doping measured in the $f = [1 - 10] \text{ GHz}$ range, as detailed in the Supplementary Information section (Fig.SI-3)

We now turn to the more general case where a significant Zener contribution is observed at high field, in both the DC transport (Fig.SI-1) and in the noise thermometry (Fig.SI-3 and insets of Figs.3), and quantified in Table-SI1. Figs.3 compare velocity flicker noise at the representative doping $n = 6 \cdot 10^{11} \text{ cm}^{-2}$ for 6 devices of the series. As seen in the figure, the bias dependencies generally deviate from the velocity-saturation bell-shape of Fig.2-b (reproduced in Fig.3-a) and described by Eq.(2). To explain this phenomenology we include in the velocity flicker a semi-empirical Zener correction to the current flicker formula in the form

$$fS_{Zener} LW = B e^{-E/E_\Lambda} \times v_Z^2 \left[\frac{E}{E_\Lambda} \right]^2, \quad (3)$$

where $B = \alpha_g/n_\Delta \sim 100 \times A$, with $\alpha_g = e^2/4\pi\epsilon_0\epsilon_h B N \hbar v_F \simeq 0.70$ the fine-structure constant

for hBN-encapsulated graphene ($\epsilon_{hBN} = 3.4$ [30]), E_Λ the decoherence field discussed in Fig.1-d (inset), and $v_Z = \frac{\sigma_Z}{en_\Delta} E_\Lambda \sim 0.01v_F$ a characteristic Zener velocity deduced from Zener conductivity σ_Z , the characteristic doping n_Δ , and E_Λ . The Zener contribution also has a bell-shape bias dependence, which is however different with a E^2 low bias dependence, a peak $fS_{Zener}LW = 4Bv_Z^2/e^2$ at $E = 2E_\Lambda$ and an exponential tail. Inspection of Eqs.(2) and (3) shows that the two contributions have similar peak amplitudes for $v_{sat}/v_Z \sim 8e^{-1} \sqrt{\frac{\pi\alpha_g}{2\alpha_0}} \simeq 36$. Their relative amplitudes depend on n_Δ and E_Λ , which enter in v_Z (A and B are simply proportional), and constitute the 2 fitting parameters used below. Their peak positions are shifted by a factor 2 for $E_{sat} \sim E_\Lambda$, in such a way that S_{Zener} prominently affects the high-field tail of the flicker noise, when S_{sat} accounts for the flicker noise onset.

Figs.3 also show fits of the velocity flicker data (orange lines) with a two-fluid model where $S_v = S_{sat} + S_{Zener}$ from Eqs.(2) and (3), using n_Δ and E_Λ as the only free parameters. The velocity-saturation (green lines) and Zener (red lines) components are displayed in each panel. A good agreement with the two-fluid model is observed with, however, some deviations at extremely high bias $E \gtrsim 0.5 \text{ V}/\mu\text{m}$ in few devices (see e.g. "InOut1" in Fig.3-b), with an high-bias noise tail at a non-zero value, possibly due to an additional spurious mechanism that remains to be clarified. The Zener contribution is tiny in the "Lyon1" device (Fig.3-a), justifying the analysis of Fig.2-b in terms of the only saturation contribution. A similar trend is observed in "Lyon2" (Fig.3-d) which is made with the same PDC-grade [29] hBN material. Other devices, fabricated with high-pressure high-temperature HPHT-grade hBN from NIMS [28], exhibit more prominent HPhP cooling in the Zener regime (see Figs.3 insets and Figs.SI-3). In these devices, single-fluid fits are unable to map the observed field dependencies, hence the justification of our 'two-fluid' (intraband saturation and interband Zener) analysis. The saturation contribution (green lines in Figs.3) is mostly responsible for the onset of flicker noise at low bias, with a slope increasing with mobility $\mu(0)$. The Zener contribution (red lines in Figs.3) becomes significant at larger bias, with a characteristic peak field at $2E_\Lambda > E_{sat}$, explaining the slower decrease of flicker noise at high bias. The amplitudes of the two contributions are comparable with, as a general trend, an intraband saturation term becoming more prominent in high-mobility devices.

We now discuss the sample-dependent parameters A (or n_Δ) and E_Λ , which are extracted from above fits and listed in Table-SI1. We obtain $A \in [2 - 7]10^{-7} \mu\text{m}^2$, corresponding to $n_\Delta \in [0.7 - 2.3]10^{12} \text{ cm}^{-2}$. These values, obtained in a broad $\mu(0) \in [2 - 15] \text{ m}^2/\text{Vs}$

mobility range, confirm the literature data $A \in [10^{-7} - 10^{-6}] \mu\text{m}^2$ reported for diffusive SiO₂-supported graphene (dark-blue rectangle in Fig. 4-a), suggesting that A is essentially impurity-scattering independent. This observation is further illustrated in the comparison between devices “Goyave2” (Table SI-1) and “AuS3” (Fig.3-f), which yield the same A in spite of a factor 7 in mobility. The similarity of flicker noise amplitude A in the impurity-dominated (linear low-mobility) and OP-phonon-dominated (non-linear high-mobility) scattering regimes, reflects one more time its universality. The characteristic field for the Zener correcting term, $E_\Lambda = 75 \pm 25 \text{ mV}/\mu\text{m}$, is quite similar for the 6 representative devices. It can be translated in terms of a Zener junction length $\Lambda = \sqrt{\hbar v_F/eE_\Lambda} = 100 \pm 15 \text{ nm}$, which shows a reduced dispersion when compared with the quite spread values of the Zener conductivity $\sigma_Z \in [0.1 - 1] \text{ mS}$.

As seen in Fig.4-a all values of A lie in the light-blue domain $A \in [2 - 6]10^{-7} \mu\text{m}^2$, where the two bounds correspond to $n_\Delta \in [0.7 - 2.3]10^{12} \text{ cm}^{-2}$. We can convert this doping range in terms of an energy range $\tilde{\Delta} = \hbar v_F \sqrt{\pi n_\Delta}$ relying on the massless dispersion of graphene. Doing so we find that $\tilde{\Delta} \in [\Delta_1, \Delta_2] = [0.09 - 0.17] \text{ eV}$ is actually bounded by the lower and upper Reststrahlen bands of hBN. These two energies have been associated in Ref.[22] to momentum relaxation (out-of-plane optical phonons of lower RS band) and energy relaxation (in-plane optical phonons of upper RS band) respectively. This finding suggests that flicker noise in high-mobility graphene does map the ambivalent nature of conductance as an admixture of momentum and energy relaxations parameters.

The correlation of flicker noise to energy relaxation is even more obvious in the Zener contribution characterized by a large $B \approx 100 A$ and the characteristic velocity $v_Z = \sigma_Z E_\Lambda / e n_\Delta$ in Eq.(3). The semi-log plot $v_Z^2(dT_N/dP)$ in Fig.4-b indeed shows a strong decrease of the Zener flicker amplitude with the thermal resistance to the hBN substrate. This is exemplified by transistor “Lyon1”, with a large thermal resistance to the hBN substrate due to weak Zener cooling, and a tiny Zener flicker amplitude. We attribute this reduced Zener cooling to the larger structural disorder in the two “Lyon”-grade hBN-based devices, where hBN is fabricated through the PDC route. As a matter of fact, hBN structural quality is essential to ensure free propagation of hyperbolic phonon polaritons in the hBN bulk; their strong backscattering/damping in “Lyon”-grade hBN devices is likely to suppress the MIR electromagnetic coupling, implying lower Zener conductivity and radiative cooling, resulting in a smaller Zener flicker noise.

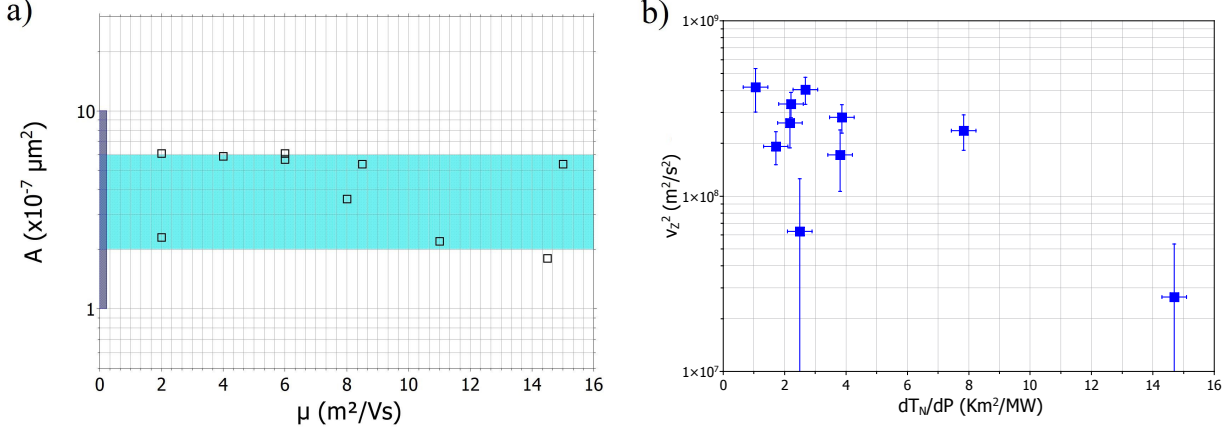


FIG. 4: Flicker-noise correlations to mobility and Zener cooling. Panel a): Noise amplitude A as function of mobility for 10 devices of the series (dots). The light-blue rectangle corresponds to our hBN-encapsulated graphene devices. Panel b): Zener-flicker amplitude v_Z^2 as function of the thermal resistance dT_N/dP in the Zener interband regime extracted from GHz noise thermometry measurements (insets of Fig.3) for the device series.

We now interpret the interband Zener term in Eq.(3), which is introduced as a correction to the intraband saturation term Eq.(2). It is characterized by a large coupling constant $\alpha_g \sim 100 \times \alpha_0$, that is affected by a field reduction factor e^{-E/E_Λ} with a nearly sample-independent characteristic field $E_\Lambda \simeq 75 \text{ mV}/\mu\text{m}$. This characteristic field can be associated to the energy scale $\varepsilon_\Lambda = \sqrt{e\hbar v_F E_\Lambda} = 7 \text{ meV}$, and length $\Lambda = \hbar v_F / \varepsilon_\Lambda = 100 \text{ nm}$ of Zener tunneling. In this interpretation, ε_Λ and Λ are the characteristic energy and length of coherent tunneling, which are limited by inelastic HPhP scattering. They control the Hooze parameter $\alpha_g e^{-E/E_\Lambda}$ in its quantum-coherent version by Handel. Note in passing that the incoherent variant of quantum theory of flicker noise involves a large reduction factor $v_F^2/c^2 \ll 1$, where c is the speed of light, with respect to the coherent one $\alpha_H = 2\alpha_0/\pi$ [9]. Further insight into this coherent mechanism requires a comprehensive theoretical approach, including geometrical antenna effects in free-light and HPhP emissions, which is still elusive and beyond the scope of the present experimental report.

The conclusion of our experimental report of α -noise in hBN-encapsulated graphene is twofold. In a first part we recover and generalize the Hooze formula for non-linear intraband transport by substituting the total current I with the differential current GV . We give

an interpretation of the constant flicker noise prefactor, previously revealed in diffusive graphene, in terms of a scattering density n_{Δ} , defined by an effective energy $\tilde{\Delta}$ interpolating between the elastic-scattering energy Δ_1 and the inelastic-scattering energy Δ_2 . In a second part, we extend the Hooge formula to include the interband transport contribution, which is prominent in high-mobility graphene at high field. We propose a compact formula, in the spirit of the Hooge-Handel interpretation of flicker noise, with a strongly enhanced interband Hooge parameter reflecting the large coupling of graphene electron-hole pairs to near-field hyperbolic phonon polaritons of hBN [23]. The graphene case corresponds to the collective strongly-inelastic variant, where IR bremsstrahlung constitutes the main energy-relaxation mechanism in the Zener regime where $\alpha_H \sim 1$. The superposition of the two flicker terms in the two-fluid α -noise analysis accounts for the observed field dependencies in a series of graphene transistors with varied IR environments. Experiment indicates that the interband coupling constant is affected by an exponential suppression factor accounting for decoherence effects in the HPhP coupling. Our observations that i) intraband Hooge parameter approaches the Handel limit $\alpha_{H,intra} = 2\alpha_0/\pi$, ii) interband parameter $\alpha_{H,inter} \sim \alpha_g$ is strongly enhanced by a factor 100, and iii) that it is sensitive to decoherence effects via the $\exp(-E/E_{\Lambda})$ factor, iv) and the correlation of flicker noise with thermal conductance to the hBN substrate, constitute four qualitative indications supporting the quantum-coherent bremsstrahlung interpretation of flicker noise. In addition, this electromagnetic coupling interpretation provides a natural explanation for the ubiquitous scatter in flicker data by ascribing it to the variability in the IR environment. In a broader perspective, our work promotes flicker noise, in complement to DC transport and noise thermometry, as a powerful semi-quantitative tool to decipher the physical mechanisms at stake in graphene transistors under extreme bias.

I. DATA AVAILABILITY

Data are available at the DOI : <https://doi.org/10.5281/zenodo.7632159>

II. AUTHOR DECLARATION

A. Conflict of interest

The authors have no conflict of interest to disclose.

B. Author contributions

AS, EB and BP conceived the experiment. AS conducted device fabrication and measurements, under the guidance of DM and MR in the early developments. TT, KW, CM, CJ and VG have provided the hBN crystals. AS, EB and BP developed the models and theoretical interpretations. AS, DM, CV, JMB, GF, CV, EB and BP participated to the data analysis. AS wrote the manuscript with assistance of EB and BP, and contributions from the coauthors.

C. Acknowledgments

Authors thank Gerbold Ménard for his critical reading of the manuscript. The research leading to these results has received partial funding from the European Union Horizon 2020 research and innovation program under grant agreement No.881603 "Graphene Core 3", and from the French ANR-21-CE24-0025-01 "ELuSeM".

-
- * Electronic address: aurelien.schmitt@phys.ens.fr
- † Electronic address: bernard.placais@phys.ens.fr
- ‡ Electronic address: emmanuel.baudin@phys.ens.fr
- ¹ A. L. McWorther, *Kingston, R. H., Ed., Semiconductor Surface Physics, University of Pennsylvania Press (1957) 1/f Noise and Germanium Surface Properties*
- ² M. A. Caloyannides, *Journ. of Appl. Phys.* **45**, 307 (1974) *Microcycle spectral estimates of 1/f noise in semiconductors*
- ³ J. B. Johnson, *Phys. Rev.* **26**, 71 (1925). *The Schottky Effect in Low Frequency Circuits*
- ⁴ F. N. Hooge, *Physics Letters A* **29**, 139 (1969). *1/f noise is no surface effect*
- ⁵ F. N. Hooge, A. M. H. Hoppenbrouwers, *Physica* **45**, 386 (1969). *1/f noise in continuous gold thin films*
- ⁶ F. N. Hooge, T. G. M. Kleinpenning, L. K. J. Vandamme *Reports on Progress in Physics* **44**, 479 (1981) *Experimental studies on 1/f noise*
- ⁷ Sh. Kogan, *Cambridge University Press (1996). Electronic noise and fluctuations in solids*
- ⁸ P. H. Handel, *Phys. Rev. Lett.* **34**, 1492 (1975) *1/f Noise—An "Infrared" Phenomenon*
- ⁹ P. H. Handel, *Phys. Stat. Sol.* **194**, 393 (1996) *Coherent and Conventional Quantum 1/f Effect*
- ¹⁰ T. M. Nieuwenhuizen, D. Frenkel, N. G. Vankampen *Physics Rev. A* **35**, 2750 (1987). *Objections to Handel quantum-theory of 1/f noise*
- ¹¹ M. B. Weissman, *Rev. Mod. Phys.* **60**, 537 (1988). *1/f noise and other slow, non-exponential kinetics in condensed matter*
- ¹² A. A. Balandin, *Nature Nanotechnol.* **8**, 549 (2013). *Low-frequency 1/f noise in graphene devices*
- ¹³ N. Mavredakis, W. Weib, E. Pallecchi, D. Vignaud, H. Happy, R. G. Cortadellac, A. Bonaccini Caliac, J. A. Garridoc, D. Jiménez, *ACS Appl. Electron. Mater.* **1**, 2626 (2019). *Velocity Saturation effect on Low Frequency Noise in short channel Single Layer Graphene FETs*
- ¹⁴ Y. M. Lin, P. Avouris, *Nano Lett.* **8**, 2119 (2008). *Strong suppression of Electrical Noise in Bilayer Graphene Nanodevices*
- ¹⁵ S. Rumyantsev, G. Liu, W. Stillman, M. Shur, A.A. Balandin, *J Phys. : Condens. Matter* **22**, 395302 (2010) *Electrical and noise characteristics of graphene field-effect transistors : ambient effects, noise sources and physical mechanisms*

- ¹⁶ S. Takeshita, S. Matsuo, T. Tanaka, S. Nakaharai, K. Tsukagoshi, T. Moriyama, T. Ono, T. Arakawa, K. Kobayashi, *Appl. Phys. Lett.* **108**, 103106 (2016) *Anomalous behavior of 1/f noise in graphene near the charge neutrality point*
- ¹⁷ A. Rehman, J.A. Delgado Notario, J. Salvador Sanchez, Y.M. Meziani, G. Cywinski, W. Knap, A.A. Balandin, M. Levinshtein, S. Rumyantsev, *Nanoscale* **14**, 7242 (2022). *Nature of the 1/f noise in graphene—direct evidence for the mobility fluctuation mechanism*
- ¹⁸ C. C. Kalmbach, F. J. Ahlers, J. Schurr, A. Maller, J. Feilhauer, M. Kruskopf, K. Pierz, F. Hohls, R. J. Haug, *Phys. Rev. B* **94**, 205430 (2016) *Nonequilibrium mesoscopic conductance fluctuations as the origin of 1/f noise in epitaxial graphene*
- ¹⁹ O. Shein-Lumbroso, J. Liu, A. Shastry, D. Segal, O. Tal, *Phys. Rev. Lett.* **128**, 237701 (2022) *Quantum Flicker Noise in Atomic and Molecular Junctions*
- ²⁰ M. Kumar, A. Laitinen, D. Cox, P. J. Hakonen, *Appl. Phys. Lett.* **106**, 263505 (2015). *Ultra low 1/f noise in suspended bilayer graphene*
- ²¹ M; A. Stolyarov, G. Liu, S. L. Rumyantsev, M. Shur, A. A. Balandin, *Appl. Phys. Lett.* **107**, 023106 (2015). *Suppression of 1/f noise in near-ballistic h-BN-graphene-h-BN heterostructure field-effect transistors*
- ²² W. Yang, S. Berthou, X. Lu, Q. Wilmart, A. Denis, M. Rosticher, T. Taniguchi, K. Watanabe, G. Fève, J.M. Berroir, G. Zhang, C. Voisin, E. Baudin, B. Plaçais, *Nature Nanotechnol.* **13**, 47 (2018). *A graphene Zener-Klein transistor cooled by a hyperbolic substrate*
- ²³ E. Baudin, C. Voisin, B. Plaçais, *Adv. Funct. Materials* **30**, 1904783 (2020). *Hyperbolic Phonon Polariton Electroluminescence as an Electronic Cooling Pathway*
- ²⁴ N. Mavredakis, W. Wei, E. Pallecchi, D. Vignaud, H. Happy, R. Garcia Cortadella, A. Bonaccini Calia, J.A. Garrido, D. Jiménez, *ACS Appl. Electron. Mater.* **1**, 2626 (2019).
- ²⁵ C. R. Dean, A. F. Young, I.Meric, C. Lee, L. Wang, S. Sorgenfrei, K. Watanabe, T. Taniguchi, P. Kim, K. L. Shepard and J. Hone, *Nat. Nanotech.* **5**, 722 (2010). *Boron nitride substrates for high-quality graphene electronics*
- ²⁶ S. Dai, Q. Ma, M. K. Liu, T. Andersen, Z. Fei, M. D. Goldflam, M.Wagner, K.Watanabe, T. Taniguchi, M. Thiemens, F. Keilmann, G. C. A. M. Janssen, S-E. Zhu, P. Jarillo-Herrero, M. M. Fogler and D. N. Basov, *Nat. Nanotech.* **10**, 682 (2015). *Graphene on hexagonal boron nitride as a tunable hyperbolic metamaterial*
- ²⁷ A. Kumar, Tony Low, K. H. Fung, P. Avouris, N. X. Fang, *Nano Lett.* **15**, 3172 (2015). *Tunable*

light-matter interaction and the role of hyperbolicity in graphene-hBN system

- ²⁸ T. Taniguchi, K. Watanabe, *Journ. of Crystal Growth* **2**, 303 (2007). *Synthesis of high-purity boron nitride single crystals under high pressure by using Ba-BN solvent*
- ²⁹ C. Maestre, Y. Li, V. Garnier, P. Steyer, S. Roux, A. Plaud, A. Loiseau, J. Barjon, L. Ren, C. Robert, B. Han, X. Marie, C. Journet, B. Toury, *2D Mater.* **9**, 035008 (2022) *From the synthesis of hBN crystals to their use as nanosheets in van der Waals heterostructures*
- ³⁰ A. Pierret, D. Mele, H. Graef, J. Palomo, T. Taniguchi, K. Watanabe, Y. Li, B. Toury, C. Journet, P. Steyer, V. Garnier, A. Loiseau, J-M. Berroir, E. Bocquillon, G. Fève, C. Voisin, E. Baudin, M. Rosticher, B. Plaçais, *Mater. Res. Express* **9**, 065901 (2022) *Dielectric permittivity, conductivity and breakdown field of hexagonal boron nitride*
- ³¹ A. Schmitt, P. Vallet, D. Mele, T. Taniguchi, K. Watanabe, E. Bocquillon, G. Fève, J.M. Berroir, C. Voisin, J. Cayssol, M. O. Goerbig, J. Troost, E. Baudin, B. Plaçais, *arXiv:2207.13400* (2022). *Mesoscopic Klein-Schwinger effect in graphene*
- ³² I. Meric, M. Y. Han, A. F. Young, B. Ozyilmaz, P. Kim, K. L. Shepard, *Nature Nanotechnol.* **3**, 654-659 (2008). *Current saturation in zero-bandgap, topgated graphene field-effect transistors*
- ³³ V. Perebeinos, P. Avouris, *Phys. Rev. B* **81**, 195442 (2010) *Inelastic scattering and current saturation in graphene*

High-field $1/f$ noise in hBN-encapsulated graphene transistors :

Supplementary Information

A. Schmitt,^{1,*} D. Mele,^{1,2} M. Rosticher,¹ T. Taniguchi,³ K. Watanabe,³ C. Maestre,⁴ C. Journet,⁴ V. Garnier,⁵ G. Fève,¹ J.M. Berroir,¹ C. Voisin,¹ B. Plaçais,^{1,†} and E. Baudin^{1,‡}

¹*Laboratoire de Physique de l'École normale supérieure,
ENS, Université PSL, CNRS, Sorbonne Université,
Université de Paris, 24 rue Lhomond, 75005 Paris, France*

²*Univ. Lille, CNRS, Centrale Lille,
Univ. Polytechnique Hauts-de-France, Junia-ISEN,
UMR 8520-IEMN, F-59000 Lille, France.*

³*Advanced Materials Laboratory, National Institute for
Materials Science, Tsukuba, Ibaraki 305-0047, Japan*

⁴*Laboratoire des Multimatériaux et Interfaces, UMR CNRS 5615, Univ Lyon,
Université Claude Bernard Lyon 1, F-69622 Villeurbanne, France*

⁵*Université de Lyon, MATEIS, UMR CNRS 5510,
INSA-Lyon, F-69621 Villeurbanne cedex, France*

Abstract

This Supplementary Information consists of a Table summarizing the geometrical and electrical parameters of the ten hBN-encapsulated graphene transistors series. It is augmented by three figures detailing the DC transport (Fig.SI-1), velocity flicker (Fig.SI-2), and noise thermometry (Fig.SI-3) of 6 representative transistors discussed in the main text.

Sample name	Gate	hBN grade	L μm	W μm	t_{hBN} nm	R_c Ω	$\mu(0)$ m^2/Vs	v_{sat} $10^6 m/s$	σ_Z mS	A nm^2	E_Λ V/mm	dP/dT_N MW/Km^2
Lyon1	Au	PDC	9	9	142	250	4	0.82	0.1	0.64	67	0.068
Lyon2	Au	PDC	5	5	142	80	8.5	0.60	0.45	0.54	99	0.402
InOut1	Au	HPHT	12.5	17.5	164	71	6	0.33	0.40	0.57	48	0.373
InOut2	Au	HPHT	20	8.5	118	300	11	0.46	0.55	0.22	94	0.128
GrS5	Graphite	HPHT	3.8	4	98	100	8	0.48	0.60	0.36	56	0.461
AuS3	Au	HPHT	11.1	11.4	90	95	15	0.42	0.40	0.54	57	0.258
Goyave2	Au	HPHT	9	13	84	89	2	0.22	0.40	0.23	86	0.585
Flicker162	Au	HPHT	7.1	7.5	150	95	14.5	0.58	1.05	0.18	81	0.952
Largevin2	Si/SiO ₂	HPHT	5.4	25.4	59	40	6	0.36	0.25	0.61	89	0.452
Coolox	Si/AlO _x	HPHT	5.3	5.8	86	140	2	0.38	0.27	0.26	140	0.262

TABLE SI-1: Geometrical and electrical properties of the 10 devices series. The first 6 devices are analyzed in Fig.3 of the main text. Basic properties include the nature of the gate electrode (Au or Graphite bottom gating, or back-gating with Si/SiO₂ or Si/AlO_x) and the origin of the hBN dielectric, the channel length L , width W , hBN dielectric thickness t_{hBN} , and contact resistance R_c . We have used two hBN grades: the high-pressure high-temperature (HPHT) from NIMS and the polymer-derived ceramic (PDC) from Lyon. The mobility $\mu(0)$, saturation velocity v_{sat} and Zener interband conductivity σ_Z are extracted from DC measurements using Eq.(1) of the main text. The next two columns contain the two flicker parameters A and E_Λ deduced from the two-fluid flicker analysis (see Fig.3 of the main text), which are discussed in the main text. The last column contains the values of the thermal resistance to the hBN substrate dT_N/dP in the Zener interband regime, extracted from thermal noise measurements.

* Electronic address: aurelien.schmitt@phys.ens.fr

† Electronic address: bernard.placais@phys.ens.fr

‡ Electronic address: emmanuel.baudin@phys.ens.fr

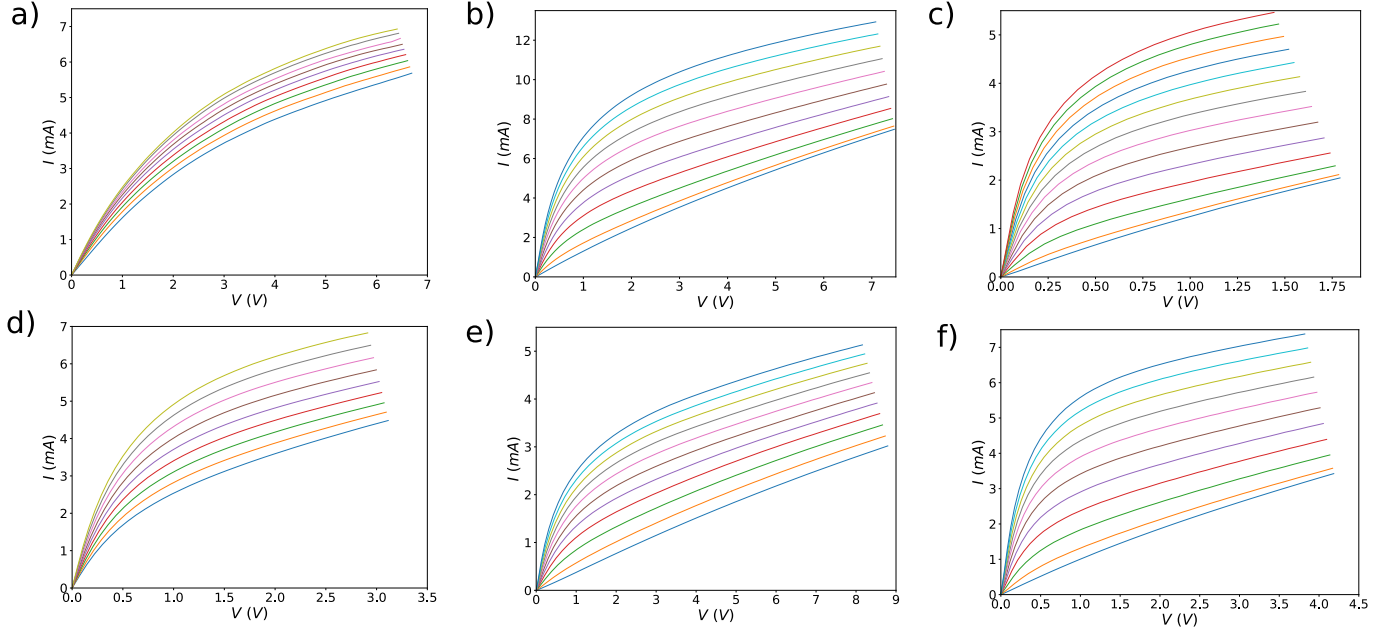


FIG. SI-1: Room temperature current voltage $I(V)$ characteristics of 6 typical high-mobility graphene transistors : Lyon1 (a), InOut1 (b), GrS5 (c), Lyon2 (d), InOut2 (e), AuS3 (f). Their geometrical and electrical parameters are described in Table SI-1. The voltage drop across the contact resistance has been subtracted to access the local electric field $E = V/L$ where L is the channel length. Main differences lie in the mobility ranging from $\mu = 4 \text{ m}^2/\text{Vs}$ for Lyon1 (panel a) to $\mu = 15 \text{ m}^2/\text{Vs}$ for AuS3 (panel f), and the Zener conductivity ranging from $\sigma_Z = 0.1 \text{ mS}$ for Lyon1 (panel a) to $\sigma_Z = 0.5 \text{ mS}$ for GrS5 (panel c).

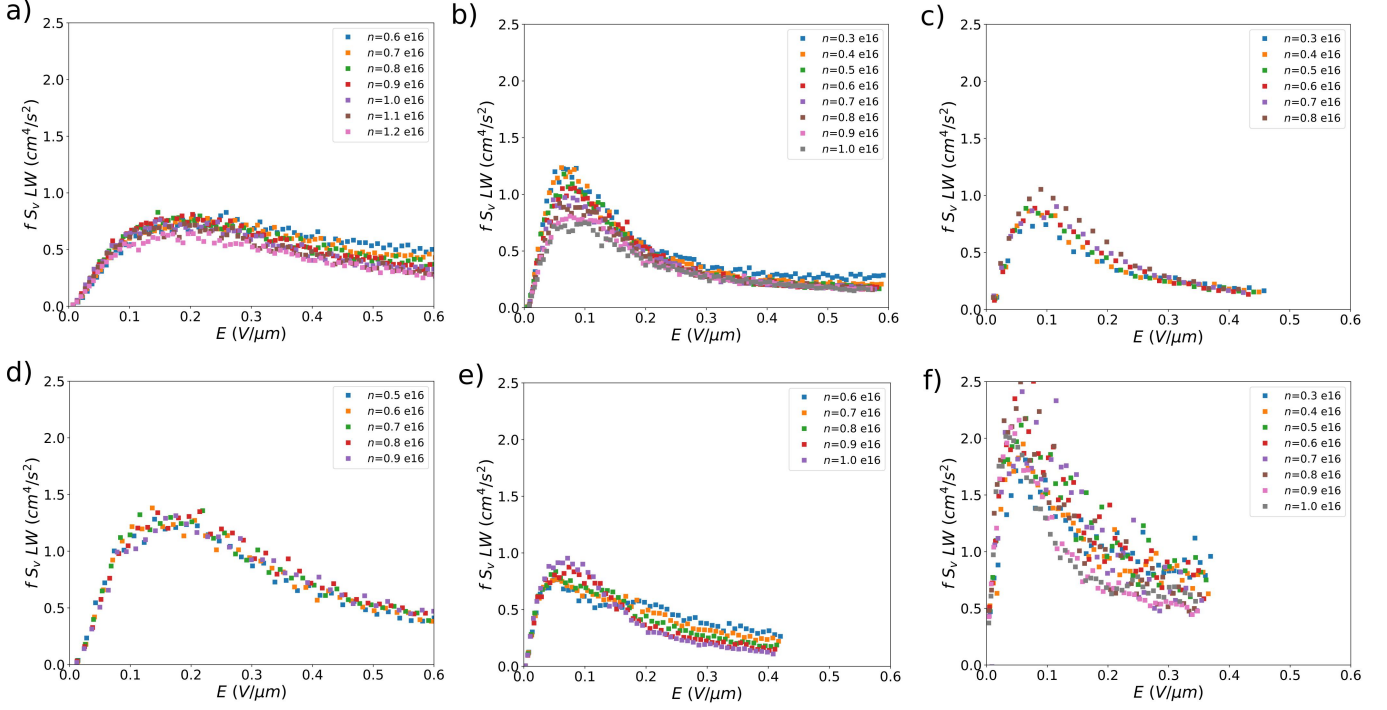


FIG. SI-2: Intensive velocity flicker noise $fS_v LW(E)$ as function of electric field $E = V/L$ for 6 typical high-mobility graphene transistors : Lyon1 (a), InOut1 (b), GrS5 (c), Lyon2 (d), InOut2 (e), AuS3 (f). Their geometrical and electrical parameters are described in Table SI-1. Velocity noise $S_v = S_I/n^2 e^2 W^2$ is deduced from the measured current noise S_I accounting for electrostatic doping n and sample width W . The figure illustrates the scaling property of the velocity flicker as discussed in the main text. Sample statistics reveal a rather universal velocity-flicker amplitude $fS_v LW = 1\text{-}2 \text{ cm}^4/\text{s}^2$, and significant variability in the electric-field dependence.

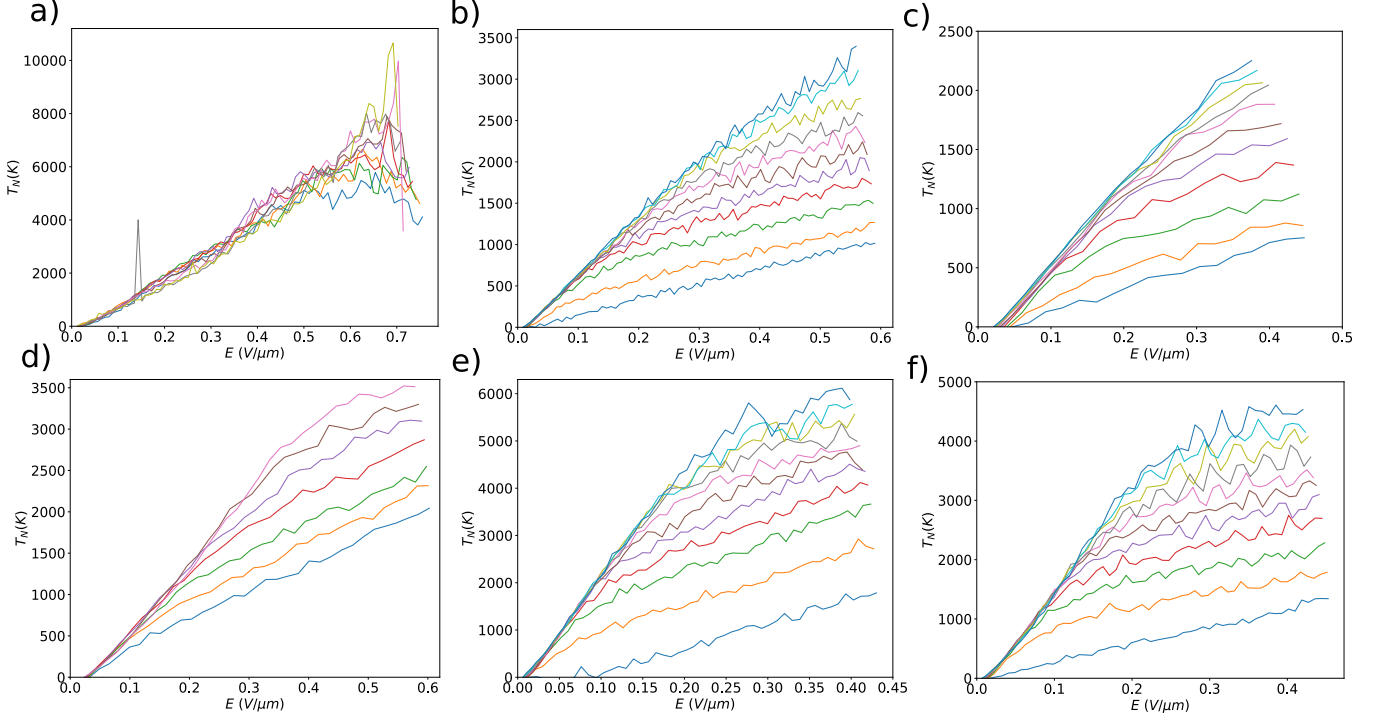


FIG. SI-3: Noise temperature $T_N(E)$ as function of electric field E for 6 typical high-mobility graphene transistors : Lyon1 (a), InOut1 (b), GrS5 (c), Lyon2 (d), InOut2 (e), AuS3 (f). Their geometrical and electrical parameters are described in Table SI-1. $T_N(E)$ is deduced from the Johnson-Nyquist noise $S_I = 4Gk_B T_N$, measured in the flicker-free 1-10 GHz microwave band, taking the DC differential conductance G as a prefactor. It characterizes the cooling pathways at stake in increasing E : the in-plane heat conduction at low E which depends on mobility, and the radiative cooling by hyperbolic phonon polariton (HPhP) emission in the hBN substrate in the Zener regime at large E . Significant sample to sample variability is observed that reflects the sensitivity of hot-electron temperature to electronic mobility at low- E and to the mobility of hBN-HPhPs at large- E with a reduced HPhP cooling in the hBN-PDC-grade transistors Lyon1 (panel a) and Lyon2 (panel d), with respect to the hBN-HPHP-grade transistors (other panels).